ASTFE American Society of Thermal and Fluids Engineers

Proceedings of the 2nd Thermal and Fluid Engineering Conference, TFEC2017
4th International Workshop on Heat Transfer, IWHT2017
April 2-5, 2017, Las Vegas, NV, USA

TFEC-IWHT2017-17459

# EFFECTS OF FILM THICKNESS ON FEMTOSECOND LASER SPALLATION AND ABLATION OF SILVER FILM

**Pengfei Ji, Yuwen Zhang***
University of Missouri, Columbia, MO 65211, USA

## ABSTRACT

*Ab initio* quantum mechanics, classical molecular dynamics and two-temperature model integrated multiscale simulation is carried out to study the effects of film thickness on the femtosecond laser spallation and ablation of silver film. At an interval of $130.7296\ nm$, five silver films with increasing thickness from $392.1888\ nm$ to $915.1072\ nm$ are simulated. The simulation results show that film thickness has close correlation with the Kelvin degree of heating of the laser irradiated silver films, which further affects the laser spallation and ablation.

**KEY WORDS:** laser ablation, laser spallation, micromachining, multiscale modeling, metal film.

## 1. INTRODUCTION

Owing to the unique merit of little collateral damage [1,2], femtosecond laser pulse processing of material has the advantage over conventional laser machining, which makes it as a widely acknowledged approach in micromachining and microfabrication. With the miniaturization of the objective material to nanoscale, plenty of challenges to the conventionally macroscopic heat transfer theories come up [3–6]. When the laser pulse duration is comparable to the timescales of ultrafast laser irradiation induced thermal and mechanical response, the factors leading to laser spallation and ablation become complex.

Considerable attentions have been drawn in studying the ultrafast laser interaction with metal film. When the laser pulse duration is in the time scale shorter than picosecond, the nonequilibrium between the laser excited hot electron subsystem and the cold lattice subsystem is significant, which cannot be solved by using the classical heat transfer methods and models [7]. Therefore, the two-temperature model was proposed to describe the nonequilibrium state [8]. In this paper, a multiscale framework integrating the quantum mechanics (QM), molecular dynamics (MD) and two-temperature model (TTM), which was constructed in our previous work [7,9,10], is to be employed to fulfill the simulation of femtosecond laser irradiation on the silver film.

## 2. SIMULATION METHOD

Five silver films with thicknesses of $392.1888\ nm$, $522.9184\ nm$, $653.6480\ nm$, $784.3776\ nm$ and $915.1072\ nm$ were simulated. A brief recall of the QM-MD-TTM integrated framework [7,9,10] is presented in this paper. The volumetric energy source $S$ is expressed in the following equation,

$$S(x,t) = \frac{0.94 J_{abs}}{t_p L} exp(-\frac{x}{L}) exp[-2.77 \frac{(t-t_0)^2}{{t_p}^2}], \quad (1)$$

where $t_p = 500\ fs$ is the laser pulse duration. $L$ equals the summation of $12\ nm$ optical penetration depth $L_{op}$ [11] and $56\ nm$ ballistic energy transport depth $L_{ba}$ [12]. $t_0 = 25\ ps$ is the temporal center point of laser pulse. Before laser irradiation, the silver film samples were prepared at $300\ K$ for $10\ ps$. The first $5\ ps$ was for the preparation of equilibrating the electron subsystem and the lattice subsystem at $300\ K$. The second $5\ ps$ was for the verification of the thermal equilibrium. The QM-MD-TTM combined simulation started at $10\ ps$. The

*Corresponding Author: zhangyu@missouri.edu

entire simulation lasted for $200\ ps$. Free boundary conditions were applied on the two surfaces of the silver film, while period boundary conditions were applied on the surfaces perpendicular to $y$- and $z$- directions. According to the TTM, the laser energy is firstly absorbed by the electron [8]. The energy equation of the electron subsystem is expressed in

$$C_e \frac{\partial T_e}{\partial t} = \nabla(k_e \nabla T_e) - G_{e-ph}(T_e - T_l) + S(x,t), \tag{2}$$

where $C_e$, $k_e$ and $G_{e-ph}$ are to be determined from QM calculation. The modeled mathematical expression are

$$\begin{cases} C_e|_{T_e} = \frac{1}{V_c}\int_{-\infty}^{\infty}\left(\frac{\partial g|_{T_e}}{\partial T_e} f|_{T_e} + g|_{T_e}\frac{\partial f|_{T_e}}{\partial T_e}\right)\varepsilon d\varepsilon \\ k_e|_{T_e} = \frac{1}{3V_c} v_F^2 \tau_e|_{T_e}\int_{-\infty}^{\infty}(\frac{\partial g|_{T_e}}{\partial T_e} f|_{T_e} + g|_{T_e}\frac{\partial f|_{T_e}}{\partial T_e})\varepsilon d\varepsilon. \\ G_{e-ph}|_{T_e} = \frac{1}{V_c}\frac{\pi\hbar k_B \lambda\langle\omega^2\rangle|_{T_e}}{g(\varepsilon_F)|_{T_e}}\int_{-\infty}^{\infty} g|_{T_e}^2(-\frac{\partial f|_{T_e}}{\partial \varepsilon})d\varepsilon \end{cases} \tag{3}$$

Under femtosecond laser excitation, $g|_{T_e}$, $g(\varepsilon_F)|_{T_e}$, $f|_{T_e}$ and $\lambda\langle\omega^2\rangle|_{T_e}$ in Eq. (3) change with different $T_e$. $g$ is the electron density of states (EDOS) and $g(\varepsilon_F)$ is the EDOS at Fermi level $\varepsilon_F$. $f$ is the Fermi-Dirac distribution. $\lambda\langle\omega^2\rangle$ is the second moment of electron-phonon spectral function. $V_c$ is the volume of unit cell. $v_F$ is the Fermi velocity. $\tau_e$ denotes the total electron scattering time. $\hbar$ and $k_B$ are reduced Planck constant and Boltzmann constant, respectively.

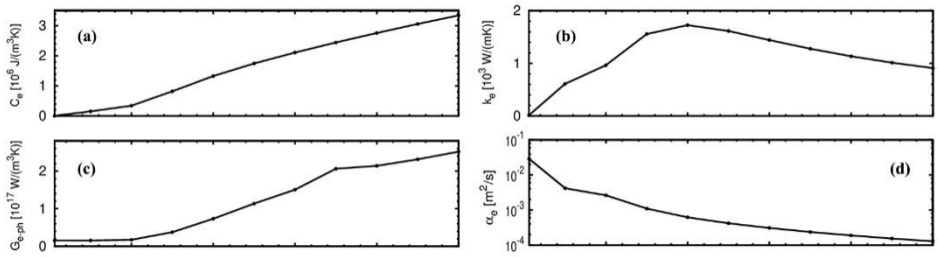


**Fig. 1** Electron temperature $T_e$ dependent (a) electron heat capacity $C_e$, (b) electron thermal conductivity $k_e$, (c) effective electron-phonon coupling factor $G_{e-ph}$, (d) electron thermal diffusivity $\alpha_e$.

Finite temperature density functional theory (FT-DFT) was implemented in calculating $g|_{T_e}$, $g(\varepsilon_F)|_{T_e}$, $f|_{T_e}$ and $\lambda\langle\omega^2\rangle|_{T_e}$. The local density approximation (LDA) with a plane wave cutoff of $28\ eV$ was adopted in computing the exchange and correlation energy. $10 \times 10 \times 10$ Monkhorst-Pack $k$-point grids were used to sample the Brillouin zone, which had been tested to meet the convergence. The finally calculated $T_e$ dependent $C_e$, $k_e$, $G_{e-ph}$, thermal diffusivity $\alpha_e$ are plotted in Fig. 1. The electron-phonon coupled heat transfer results in an addition force acting on the nuclei. The equation of atomic motion in MD simulation is expressed in the following equation

$$m_i \frac{d^2 \boldsymbol{r_i}}{dt^2} = -\nabla U + \frac{E_{e-ph}}{\Delta t_{MD}} \frac{m_i \boldsymbol{v_i^T}}{\sum_{j=1}^{N_V} m_j \left(\boldsymbol{v_j^T}\right)^2}, \tag{4}$$

where $m_i$, $\boldsymbol{r_i}$ and $v_i^T$ are the mass, position and thermal velocity of atom $i$, respectively. The interatomic force acting on the nuclei is $-\nabla U$. Here $U$ is interatomic potential [13]. $N_V$ is the number atoms in each computational cell. In each MD time step $\Delta t_{MD}$, the thermal energy transporting from the electron subsystem to the lattice subsystem is $E_{e-ph}$. The QM-MD-TTM integrated framework is constructed by combing Eqs. (1)-(4). The simulation code is developed as an extension of the ABINIT package [14] and the TTM part in the IMD [15]. During the QM-MD-TTM integrated simulation, the time steps $\Delta t_{MD}$ and $\Delta t_{FDM}$ were set as $1 fs$ and $0.005\ fs$ to meet the von Neumann stability criterion.

## 3. RESULTS AND DISCUSSIONS

When $J_{abs}$ is $0.3\ J/cm^2$, femtosecond laser induced spallation and ablation were seen for the cases with film thicknesses of $392.1888\ nm$ and $522.9184\ nm$. Whereas, only ablation was seen for the other three cases with film thicknesses of $653.6480\ nm$, $784.3776\ nm$ and $915.1072\ nm$.

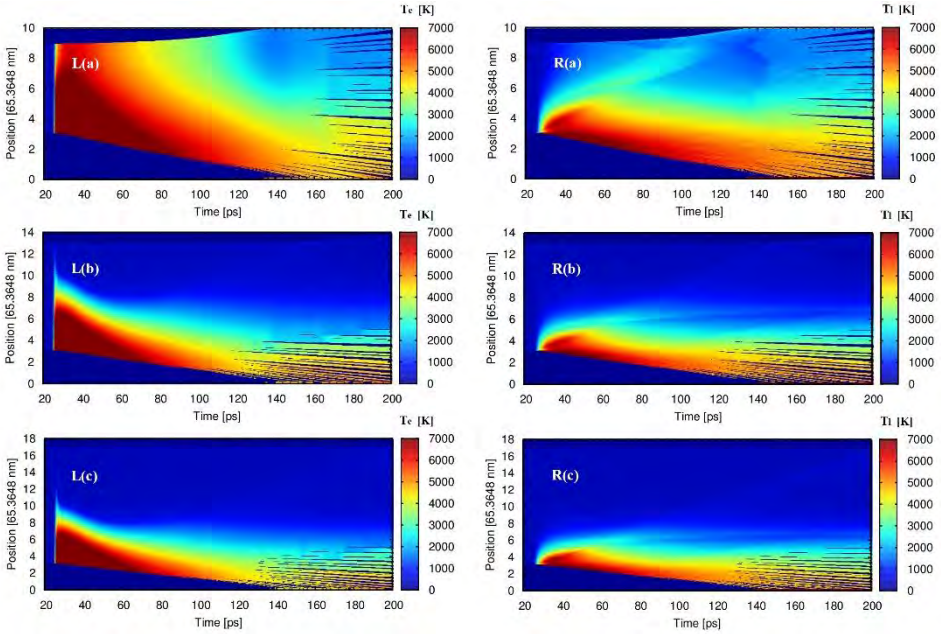


**Fig. 2** The temporal and spatial distribution of electron temperature $T_e$ (left panel) and lattice temperature $T_l$ (right panel) for the silver film thickness of (a) 392.1888 $nm$; (b) 653.6480 $nm$ and (c) 915.1072 $nm$.

The distributions of $T_e$ for the cases with thicknesses of 392.1888 $nm$, 653.6480 $nm$ and 915.1072 $nm$ are plotted in Fig. 2L. At 27 $ps$, $T_e$ at the rear surface of the silver film are 5071.58 $K$, 354.89 $K$ and 303.01 $K$, respectively. Therefore, it can be concluded that even though the laser fluence increases, the silver film with thickness greater than 653.6480 $nm$ is sufficient to keep the rear side of the film being not significantly heated. At 170 $ps$, the silver film in Fig. 2L(a) has been totally split into several segments. It should be noted that $T_e$ of these segments from the front surface to the rear surface range from 4,533.94 $K$ to 1693.15 $K$.

**Table 1** Film thickness dependent spallation depth $L_{spa}$ and ablation depth $L_{abl}$

| Film Thickness ($nm$) | $L_{spa}$ ($nm$) | $L_{abl}$ ($nm$) |
|---|---|---|
| 392.1888 | 451.0171 | 261.4592 |
| 522.9184 | 535.9914 | 210.8015 |
| 653.6480 | N/A | 137.2661 |
| 784.3776 | N/A | 133.9978 |
| 915.1072 | N/A | 130.7296 |

The distributions of $T_l$ for the above three cases are plotted in Fig. 2R. With the increase of the film thickness, the depth of heated region changes a lot. $T_l$ at 80 $ps$ at $x = 457.5536\ nm$ for the three cases Fig. 2R are 2,817.66 $K$, 1575.14 $K$ and 1,579.81 $K$, respectively, which reveals that when the film thickness is greater than 653.6480 $nm$, the effect of film thickness for laser heating with is no longer a dominate factor. As seen in Fig. 2R(b), a $T_l$ line appears since 70 $ps$ and develops to the deeper regions with the evolution of time. The $T_l$ line will be discussed in detail from the density distribution in Fig. 2R. With the continuous progress of simulation, $T_l$ gradually becomes in consistent with $T_e$ in Fig. 2L. The splits generated front the front surfaces of the cases in Figs. 2R(b) and 2R(c) show values above boiling point 2435.15 $K$ of silver [16]. Explosive boiling are found from the front surface when $25\ ps < t < 80\ ps$, which is verified by $T_l$ show values greater than 0.9 times of the critical temperature 6,410.15 $K$ of silver [16]. Due to the limits to the current QM-MD-TTM simulation, the generation of plasma is not included in this paper.

Table 1 presents the spallation depth $L_{spa}$ and ablation depth $L_{abl}$ for the cases with $J_{abs} = 0.3\ J/cm^2$. Laser spallation is also seen for the film with thickness of 522.9184 $nm$ during the 200 $ps$ simulation time. Laser spallation damages the silver films (with thicknesses of 392.1888 nm and 522.9184 nm) into a few small

segments. For the silver film without laser spallation, steady surface is seen from the front side of the remained silver film.

## 4. CONCLUSIONS

The dependence of film thickness on femtosecond laser irradiation has been investigated in this paper. The simulation takes advantages of the highly accurate QM determination of the electron thermophysical properties, the detailed description of the laser pulse induced atomic motion and phase change process, as well as the inclusion of energy evolution of the laser energy excited electron subsystem in continuum. The coexistence of ablation and laser spallation results in the damage of the silver film into several small segments.

## ACKNOWLEDGMENT

Support for this work by the U.S. National Science Foundation under grant number CBET- 133611 is gratefully acknowledged.

## REFERENCES

[1] Stuart, B., Feit, M., Herman, S., Rubenchik, A., Shore, B., and Perry, M., "Nanosecond-to-femtosecond laser-induced breakdown in dielectrics," Phys. Rev. B, 53(4), pp. 1749–1761, (1996).
[2] Sudrie, L., Couairon, a, Franco, M., Lamouroux, B., Prade, B., Tzortzakis, S., and Mysyrowicz, A, "Femtosecond laser-induced damage and filamentary propagation in fused silica.," Phys. Rev. Lett., 89(18), pp. 186601, (2002).
[3] Cahill, D. G., Ford, W. K., Goodson, K. E., Mahan, G. D., Majumdar, A., Maris, H. J., Merlin, R., and Phillpot, S. R., "Nanoscale thermal transport," J. Appl. Phys., 93(2), pp. 793, (2003).
[4] Cahill, D. G., Braun, P. V., Chen, G., Clarke, D. R., Fan, S., Goodson, K. E., Keblinski, P., King, W. P., Mahan, G. D., Majumdar, A., Maris, H. J., Phillpot, S. R., Pop, E., and Shi, L., "Nanoscale thermal transport. II. 2003–2012," Appl. Phys. Rev., 1(1), pp. 011305, (2014).
[5] Ji, P., and Zhang, Y., "First-principles molecular dynamics investigation of the atomic-scale energy transport: From heat conduction to thermal radiation," Int. J. Heat Mass Transf., 60(1), pp. 69–80, (2013).
[6] Ji, P., Zhang, Y., and Yang, M., "Structural, dynamic, and vibrational properties during heat transfer in Si/Ge superlattices: A Car-Parrinello molecular dynamics study," J. Appl. Phys., 114(23), pp. 234905, (2013).
[7] Ji, P., and Zhang, Y., "Femtosecond laser processing of germanium: an ab initio molecular dynamics study," J. Phys. D. Appl. Phys., 46, p. 495108, (2013).
[8] Anisimov, S. I., Kapeliovich, B. L., and Perel-man, T. L., "Electron emission from metal surfaces exposed to ultrashort laser pulses," J. Exp. Theor. Phys., 39(2), pp. 375–377, (1974).
[9] Ji, P., and Zhang, Y., "Continuum-atomistic simulation of picosecond laser heating of copper with electron heat capacity from ab initio calculation," Chem. Phys. Lett., 648, pp. 109–113, (2016).
[10] Ji, P., and Zhang, Y., "Ab initio determination of effective electron–phonon coupling factor in copper," Phys. Lett. A, 380(17), pp. 1551–1555, (2016).
[11] Bäuerle, D., Laser Processing and Chemistry, (2011).
[12] Ashcroft, N. W., and Mermin, N. D., "Solid state physics," Holt, Rinehart and Winston, (1976).
[13] Sheng, H. W., Kramer, M. J., Cadien, A., Fujita, T., and Chen, M. W., "Highly optimized embedded-atom-method potentials for fourteen FCC metals," Phys. Rev. B, 83(13), pp. 134118, (2011).
[14] Gonze, X., Amadon, B., Anglade, P.-M., Beuken, J.-M., Bottin, F., Boulanger, P., Bruneval, F., Caliste, D., Caracas, R., Côté, M., Deutsch, T., Genovese, L., Ghosez, P., Giantomassi, M., Goedecker, S., Hamann, D. R. R., Hermet, P., Jollet, F., Jomard, G., Leroux, S., Mancini, M., Mazevet, S., Oliveira, M. J. T. J. T., Onida, G., Pouillon, Y., Rangel, T., Rignanese, G.-M., Sangalli, D., Shaltaf, R., Torrent, M., Verstraete, M. J. J., Zerah, G., and Zwanziger, J. W. W., "ABINIT: First-principles approach to material and nanosystem properties," Comput. Phys. Commun., 180(12), pp. 2582–2615, (2009).
[15] Stadler, J., Mikulla, R., and Trebin, H., "IMD: A software package for molecular dynamics studies on parallel computers," Int. J. Mod. Phys. C, 8(5), pp. 1131–1140, (1997).
[16] Haynes, W. M., "Melting , Boiling , Triple , and Critical Points of the Elements," CRC Handbook of Chemistry and Physics, 97th Edition, pp. 4–116– 4–118, (2016).